Short-term solar forecasting performance of popular machine learning algorithms

Alex Dobbs

Office of Science, Community College Internship Program

Colorado School of Mines, Golden, CO

National Renewable Energy Laboratory

Golden, Colorado

August 4, 2017

Prepared in partial fulfillment of the requirement of the Department of Energy, Office of Science's Community College Internship Program under the direction of Anthony Florita at the National Renewable Energy Laboratory.

Participant: Alex Dobbs

Research Advisor: Anthony Florita
Anthony Florita

ABSTRACT

A framework for assessing the performance of short-term solar forecasting is presented in conjunction with a range of numerical results using global horizontal irradiation (GHI) from the open-source SURFRAD data network. A suite of popular machine learning algorithms is compared according to a set of statistically distinct metrics and benchmarked against the persistence-of-cloudiness forecast and a cloud motion forecast. Results show significant improvement over the benchmarks with tradeoffs among the machine learning algorithms dependending on the desired error metric. Training inputs include time series observations of GHI for a history of years, historical weather and atmospheric measurements, and corresponding date and timestamps, such that training sensitivities may be inferred. Prediction outputs are GHI forecasts for one, two, three, and four hours ahead of the issue time, and are made for every month of the year for seven locations. Photovoltaic (PV) power and energy outputs can then be made using the solar forecasts to better understand power system impacts.

I. INTRODUCTION

The integration of high levels of solar power into the grid poses a significant challenge to grid operators due to the uncertainty and variability of solar genereration. Improving solar irradiance forecasting will ease the ramping demands of back up generators for the grid. One of the goals of the Power Systems Design & Studies (PSDS) group within the Energy Systems Integration Facility (ESIF) at the National Renewable Energy Laboratory (NREL) is to research various methods to improve solar forecasting. Machine learning is one of the newest approaches to this challenge and shows promise to make large improvements to short-term solar forecasting.

Accurate forecasting of solar energy production for unit commitment can reduce solar generation uncertainty, which translates to significant savings. A study by Lew et al. finds that $5 billion savings could be achieved on the Western Electricity Coordinating Council (WECC) per year by integrating solar and wind forecasts into unit commitments.[1] Inman et al. provides a comprehensive review of state of the art methods in solar forecasting, which primarily focuses on averaged rather than instantaneous forecasts.[2] Lorenz et al. show that for short-term forecasts, accuracy is greatly improved by applying model output statistics (MOS) to Numerical Weather Prediction (NWP) methods.[3] A variety of regression approaches have been applied to improve short-term solar forecasting.[4-8] For 15-minute to four-hour ahead forecasts, hybrid machine learning approaches have achieved significant improvements over the traditional NWP models.[9] A study by Perez et al. finds that the use of inputs such as satellite data improves the accuracy of short-term forecasts at several surface radiation (SURFRAD) sites.[10] Other studies such as Gordon et al. incorporate other exogenous observations such as relative humidity and cloud cover, which are utilized by the forecasting methodologies to improve forecasting accuracy.[11]

The method developed in this paper utilizes irradiance and exogenous weather time series data from seven publicly available weather stations in the surface radiation (SURFRAD) network, and uses different machine learning (ML) algorithms to predict solar irradiance forecasts one, two, three, and four hours ahead. This paper begins by describing the available data and the preprocessing techniques that were applied in this study. A brief overview of the ML forecasting methods is then given, followed by results and discussion comparing the performance of the ML models against the benchmarks and against each other. Finally, concluding remarks and suggestions for future research will be presented. The work presented in this paper was completed at the Department of Energy's (DOE) National Renewable Energy Laboratory (NREL).

II. PROCESS

A. Preprocessing input data

The methodologies developed in this paper were trained and tested on data from the SURFRAD observation sites in Desert Rock, NV; Fort Peck, MT; Boulder, CO; Sioux Falls, SD; Bondville, IL; Goodwin Creek, MS; and Penn State, PA. Each site has 11 years of weather measurements, at one-minute resolution from 2009 to 2014, and at three-minute resolution from

2004 to 2008. This array of sites offers climatically different weather situations. Global horizontal irradiance (GHI) at the SURFRAD sites is best represented by the *global downwelling* solar measurements. The clear sky GHI at time *t* is denoted by GHI_{clear}^{t} and represents the theoretical GHI at time *t* assuming zero cloud coverage, and is computed using the Bird model.[12] Clear sky index is a metric of cloud cover that has been used extensively in forecasting literature.[13-15] The clear sky index at time *t* denoted by $Kt_i^{(t)}$ is the ratio between the instantaneous observed GHI^t and the theoretical maximum GHI_{clear}^{t}. Current time, temperature, relative humidity, wind speed, wind direction, pressure, thermal infrared, GHI^t, GHI_{clear}^{t}, and $Kt_i^{(t)}$, are used as independent variables for the input training vectors.

Rather than training on the observed instantaneous GHI values at the one, two, three, or four-hour ahead forecast horizons (*f.h.),* which may not be representative of the *most probable* $GHI^{f.h.}$, the ML models are trained on the average clear sky index for the hour ending at the *f.h.*. The averaged hourly clear sky index ending at time *f.h.* is denoted by $Kt_a^{(f.h.)}$, as in

$$\frac{\sum_{s=f.h.-60}^{f.h} Kt_i^{(s)}}{60} \qquad \text{Equation 1}$$

$Kt_a^{(f.h.)}$ is used as the dependent variable when training each model, and the models are then used to predict $Kt_a^{(f.h.)}$ when given unseen test vectors. The forecasted $Kt_a^{(f.h.)}$ value is then multiplied by $GHI_{clear}^{f.h.}$ from the Bird model to predict $GHI^{f.h.}$, as in

$$GHI_{prediction}^{f.h.} = Kt_a^{(f.h)} \cdot GHI_{clear}^{f.h.} \qquad \text{Equation 2}$$

This ML forecast is finally compared to the testing input's corresponding $GHI_{observed}^{f.h.}$ from the SURFRAD data to assess forecasting accuracy.

Data was partitioned by month and any entries with missing or misreported data were removed. All nighttime entries with current or future GHI readings below 20 W/m^2, were removed to improve the performance of the ML algorithms. Each ML algorithm has many hyper-parameters that can be tuned and these internal parameters were set using a grid search method. Predictions were made for each forecasting situation at a frequency equal to the forecast horizon time span. For example, when forecasting GHI for three hours ahead, the ML models made predictions at three-hour intervals every day of the month for all daylight hours.

B. Description of forecasting methods

1. Persistence of cloudiness

Persistence forecasts use the current cloud cover to predict the future GHI. The forecast horizon's clear sky index is set to the current clear sky index at t and multiplied by $GHI_{clear}^{f.h.}$. This simple model is most effective for very short-term forecasts (e.g. minute ahead range), but can also be used to make one to four-hour ahead forecasts. Persistence forecasts were provided as a benchmark for the forecasts performed by ML methods in this study.

2. Support vector machines

Support Vector Machines (SVMs) have been used in many solar forecasting applications, and have been shown to work well in conjunction with other methods.[16-18] SVM regression estimates a target function based on the training instances. The output observations are assumed to take the form of $y_i = (w_i \bullet x_i) + b$, where y_i is the output observation for training instance i, x_i is the input training vector for instance i, w_i is a weight vector which defines the functional form, and b is the bias constant. SVMs operate by transforming a non-linearly separable feature space into a multi-dimensional space where variables can be seperated by a 3-D *hyperplane*. SVMs map the original data into this higher dimensional space using a technique known as the kernel trick, which allows for different perspectives on the data and makes linear relations more apparent. The final objective is to minimize the deviation errors between the output observation y_i, and the linear functional form $= (w_i \bullet x_i) + b$, while maximizing the margin of space on either side of the hyperplane.

3. Artificial neural networks

Artificial Neural Networks (ANNs) are one of the most popular machine learning methods used in solar forecasting.[19-21] ANNs operate as computational models of the neural networks found in the human brain. They contain layers of nodes with connections between nodes in adjacent layers. The input layer consists of one node for each input signal such as current time, temperature, GHI, etc. The output layer has a single output node for the corresponding $GHI^{f.h.}$. Between the input and output layers are one or more hidden layers, which contain a pre-determined number of nodes. Each node receives a weighted sum of input from the signals in the previous layer, and applies an activation function to the weighted sum. The weight of each connection is akin to the strength of neural connections in the brain. The output from the network is compared to the known training output value, and back propogation is performed to adjust the weights between the network's nodes. This process is repeated until proper weights have been determined for the training data and the network can then be used to test unseen data.

4. Random forests

A Random Forest (RF) machine learning algorithm, is a forest made of an ensemble of decision trees. RFs have been used in solar forecasting in several studies.[22-24] Each decision tree directs input through several classification and regression decision nodes. Each node splits into two possible branches, or outcomes, with each branch leading to another node. The process repeats until a terminal node is reached and an output value is connected to the given inputs. Performance of a single decision tree can be improved by training multiple regression trees with different structures and then averaging their predictions. RFs add random feature selection at each node for greater diversity in the decision tree models. Individual decision trees may have a bias due to their specific feature selection and structure but a RF averages over all the decision trees, significantly minimizing the error bias for the final prediction.

5. Gradient boosting

Gradient Boosting (GB) is a less common ML approach to solar forecasting, and is used in this study to extend the RF approach.[25] As with RF, GB uses an ensemble of decision trees to make a more accurate prediction. In GB, however, trees are added to the ensemble incrementally in the training phase to correct for any residuals occuring in existing decision trees. These residuals are the negative gradients that quantify the amount of variability between a prediction and the expected outcome of the predictive function based on the independent variables of a single training instance. Adding trees one at a time allows each new tree to be specifically trained to improve an already trained ensemble, as opposed to the RF process of randomly adding nodes to new trees to provide for a better average.

C. Situation dependent, multi-model blending

One, two, three, and four-hour ahead forecasts were generated for all 12 months at all seven SURFRAD sites. The developed code was run 336 times to model each unique forecasting situation. Each run trained all four ML algorithms on pre-processed data for the desired month from the years 2004-2008 and 2010-2014. After the models were built they were tested on unseen data from 2009 and forecasts were made for the desired forecast horizon.

D. Validation metrics

A suite of validation metrics is used to compare the forecast accuracy of different methodologies and situations in this study. A thorough discussion of different validation metrics is covered by Zhang et al. for comparing N observed GHI values $\vec{G}$ with the N forecast values $\vec{H}$.[26] Root Mean Square Error (RMSE) and Mean Absolute Error (MAE) are commonly used metrics that measure the difference between the forecasted and actual GHI values. The RMSE metric is commonly used to evaluate the overall accuracy of forecasts and penalizes large forecasting errors with its square order. The MAE metric is also appropriate for evaluating errors through the entire forecasting period, and is widely used in regression problems and by the renewable energy industry. It does not penalize large forecast errors as much as the RMSE metric. Smaller values of these validation metrics indicate a higher forecasting accuracy.

III. RESULTS & DISCUSSION

A. ML forecasts vs. benchmark methods

To calibrate this study against existing literature, forecasts were made for the same one, two, three, and four-hour ahead forecast horizons as Perez et al. study.[27] Their study tested the period from August 23, 2008 through August 31, 2009. Limitations arose in this study from the algorithms' inabilities to predict on the years before 2009, those years consisting of three-minute data resolution, which caused this study to use a slightly different testing period. Instead, this study made predictions over the period from January 1, 2009 to December 31, 2009. Seasons were partitioned into four three-month periods beginning with January 1st through March 31st.

Results are compared to both Perez's forecasts of a slightly different time period and to the persistence of cloudiness forecasts made for the same January 1, 2009 through December 31, 2009 time period.

Table 1 in Appendix B shows the RMSE values for ML predictions made in this study, Perez's forecasts, and the persistence of cloudiness forecasts. The values in the yellow columns in Table 1 are composed by taking the best performing machine learning algorithm per month and compiling these into seasonal and yearly results. The ML models employed in this study outperformed the persistence of cloudiness forecasts in every situation with average RMSE values of 92.36 W/m^2 and 122.12 W/m^2, respectively. This study outperformed Perez's forecasting methodology, which was tested on a different period, with average RMSE values of 92.36 W/m^2 and 108.29 W/m^2, respectively.

Comparing the performance of forecasting methods is also discussed using the relative frequency (rounded) that a given technique had in producing the lowest error. This study outperformed Perez's method on a seasonal basis for one and four-hour ahead forecasts in 86% and 57% of tests, respectively, based on RMSE values. However, their results outperformed this study for two and three-hour ahead forecasts in 57% and 61% of forecasts, respectively. The Perez forecasts also outperformed this study in 68% of winter and 57% of spring seasonal forecasts, while the ML models outperformed the Perez forecasts in 75% and 79% of all situations for the summer and fall seasons, respectively. When broken down by geographic location, this study outperformed Perez et al. in Boulder, Fort Peck, Desert Rock, and Bondville with respective relative frequencies of 75%, 94%, 63%, and 53% across all tests. Their study outperformed this study when forecasting across all situations in Goodwin Creek, Penn State, and Sioux Falls 75%, 56%, and 56% of the time. These relative frequencies only take into account the number of times that one method outperformed the other and do not consider the margin of difference, in W/m^2, between competing forecasts.

Relative frequencies are useful to show which method works best in individual forecasting situations but are not ideal for assessing a method's overall ability to minimize forecasting errors across all situations. Figure 1 in Appendix C compares the ML forecasts' RMSE values with the two benchmark forecasts, Perez and persistence, for all SURFRAD sites. The graphs show how forecasting errors tend to increase as the forecast horizon extends in time. The relative strength of the Perez two and three-hour ahead forecasts over the ML models is especially apparent in the graphs for Bondville, Goodwin Creek, and Penn State. Comparisons are also made by showing the percentage improvement, defined as the difference between the RMSE of the ML forecast and the RMSE of the benchmark forecast divided by the RMSE of the benchmark. The greatest improvement across all situations occurs in Fort Peck where the suite of ML algorithms demonstrates a 28.8% improvement over the Perez forecasts' average RMSE values, followed by a 25.7% improvement in Boulder. Improvements over Perez forecasts's RMSE averages are made in Desert Rock, Sioux Falls, Penn State, Bondville, and Goodwin Creek by 21.5%, 10%, 6.4%, 4.8%, and 0.7%, respectively. It is interesting to note that this study shows the largest improvements in RMSE scores for Boulder, Fort Peck, and Desert Rock. These

three sites are located at the highest elevations and are the three westernmost locations in the SURFRAD network. ML forecasts outperform the RMSE results from the persistence of cloudiness forecasts for all sites as well. They show the greatest improvement in the four locations situated eastward of mountain ranges or other orographic features: Boulder (25.3%), Desert Rock (30.7%), Penn State (26.3%), and Fort Peck (27.2%).

B. Performance of ML algorithms against each other

Table 2 in Appendix B compares the four ML models used in this study against each other by showing the relative frequency (rounded) of each algorithm's ability in producing the lowest RMSE values in the listed forecasting situations. There were 84 forecasting situations for each of the four forecast horizons (12 months per seven sites), 84 situations for the seasonal forecasts (three months per seven sites for four forecast horizons), and 48 situations for the geographic forecasts (12 months per four forecast horizons) in this study. The ANN algorithm was the top performer in each of these situational categories and produced the lowest error value in 41.1% of the 336 forecasting situations, based on the RMSE metric. The SVM algorithm performed equally well in Fort Peck, and when the seasons are broken down by month, SVM outperformed ANN during all April forecasts by 42% to 32%. The RF and SVM algorithms performed almost equally well when considering all forecast situations.

Table 3 in Appendix B is similar to Table 2 except that it shows the relative frequency of each model's ability to produce the lowest MAE values in each forecasting situation. The SVM algorithm produced the lowest MAE values in all types of forecasting situations more often than any of the other ML models, though it tied ANN when making three-hour ahead forecasts. It was the top performer in more situations according to the MAE metric than the ANN was when considering the RMSE metric. The SVM performed best most often in one-hour forecasts and approached lower relative frequencies as the forecast horizon extended in time.

IV. CONCLUSIONS & FUTURE WORK

This paper assessed the performance of machine learning techniques and their validity in improving short-term solar forecasting. The machine learning approach was compared to other forecasting methods, and individual machine learning algorithms were compared against each other. ML forecasts generated lower average RMSE values than a cloud motion forecasting method for all seven sites, with the biggest improvements for the three sites at the highest elevations and westernmost locations in the SURFRAD network. They also outperformed persistence of cloudiness forecasts at all seven sites, with the greatest improvements at the four locations situated downwind from large orographic features. The ML forecasts had the lowest RMSE more often than the cloud motion method across all summer and fall seasonal forecasts, as well as for one and four-hour ahead forecasts. Assessing the performance of the four algorithms against each other did not reveal any strong situation dependent sensitivities, as each algorithm was capable of making the best forecast in the various forecasting situations though some less than others. However, either SVMs or ANNs most often led to the lowest forecasting

errors depending on the error metric used. ANN was the preferred algorithm if minimizing the largest point forecast errors is the greatest concern, according to the RMSE metric. However, SVM was the best performer if minimizing the average absolute difference, MAE, is top priority.

This solar irradiance forecasting methodology can be extended by increasing the forecast horizon resolutions from hourly increments to five-minute increments, allowing for more dynamic time series information about upcoming ramping events. Further work is needed to fine-tune each ML algorithm, and future research should also look into optimizing ML hyper-parameters for each situation dependent forecast. Improved forecasts will help facilitate higher penetrations of solar energy into the grid by providing increased grid reliability and minimizing costs associated with ramping events.

V. ACKNOWLEDGEMENTS

I would like to thank Anthony Florita, Tarek Elgindy, and Bri-Mathias Hodge for their support and guidance throughout this project. I would also like to thank the workforce development team at NREL, the CCI program, and the Office of Science. This work was supported in part by the U.S. Department of Energy, Office of Science, Office of Workforce Development for Teachers and Scientists (WDTS) under the Community College Internships Program (CCI).

VI. APPENDICES

Appendix A: Equations

RMSE is defined as

$$\sqrt{\frac{1}{N}\sum_{i=1}^{N}(G(i) - (H(i))^2} \qquad \text{Equation 3}$$

MAE is defined as

$$\frac{1}{N}\sum_{i=1}^{N}|G(i) - H(i)| \qquad \text{Equation 4}$$

for comparing N observed GHI values $\vec{G}$ with the N forecast values $\vec{H}$.

Appendix B: Tables

Table 1: Yearly and Seasonal RMSE Metric Summary

	Forecast Horizon	Boulder			Bondville			Goodwin Creek			Fort Peck			Desert Rock			Penn State			Sioux Falls		
		ML	PC	PZ	ML	PC	PZ	ML	PC	PZ	ML	PC	PZ	ML	PC	PZ	ML	PC	PZ	ML	PC	PZ
ALL YEAR	1 hour	74	104	120	62	83	85	71	96	80	56	79	94	52	76	80	67	96	86	52	74	68
	2 hour	108	142	139	98	118	98	103	130	101	81	110	106	72	103	88	97	132	99	81	106	84
	3 hour	123	161	154	116	135	112	125	146	114	94	126	123	83	116	96	114	151	113	96	126	102
	4 hour	125	169	166	121	143	122	120	152	127	93	130	132	82	122	104	117	157	124	103	136	115
WINTER	1 hour	55	74	64	51	66	60	58	87	48	36	53	107	45	66	46	53	72	57	41	62	48
	2 hour	81	98	71	82	104	66	98	128	59	52	74	105	63	92	48	79	102	57	65	96	58
	3 hour	96	113	81	104	117	74	122	146	66	62	84	109	75	106	59	91	122	59	82	117	69
	4 hour	87	119	85	105	123	81	111	147	70	58	84	112	84	107	70	96	127	65	89	122	78
SPRING	1 hour	97	143	125	84	114	93	94	127	92	75	108	110	71	108	86	84	117	83	66	94	69
	2 hour	137	195	141	133	154	109	125	171	122	110	149	124	106	147	95	119	161	99	103	133	90
	3 hour	170	218	157	147	178	123	159	190	144	129	174	141	120	155	111	143	183	118	124	156	107
	4 hour	162	228	170	159	189	137	145	202	164	134	186	148	115	171	115	145	190	137	131	171	126
SUMMER	1 hour	96	136	143	76	97	100	88	119	92	81	101	91	48	71	99	88	125	112	67	90	80
	2 hour	137	185	175	111	134	115	121	151	113	110	143	109	64	85	110	122	170	127	99	129	98
	3 hour	144	211	189	135	153	129	135	168	120	125	164	129	70	105	111	140	194	142	112	155	120
	4 hour	175	222	204	138	169	138	139	175	129	122	173	142	74	118	124	138	208	152	118	168	129
FALL	1 hour	46	63	85	35	56	58	44	50	55	34	52	59	43	60	55	45	71	60	35	48	49
	2 hour	78	92	97	67	80	68	67	70	66	52	73	67	57	87	62	69	96	71	57	67	54
	3 hour	81	103	110	76	90	84	83	81	81	59	81	83	65	97	69	80	104	76	65	76	64
	4 hour	75	107	120	81	143	89	87	81	94	58	78	88	56	94	72	89	102	83	74	81	80

ML (yellow columns): Forecasts made by machine learning methods.

PC (white columns): Benchmark forecasts made by persistence of cloudiness method.

PZ (blue columns): Benchmark forecasts made by the Perez et al. cloud motion method.

Table 2: Relative Frequencies of ML Models per RMSE Metric

Forecast Situation	RF	SVM	ANN	GBM
1-hour ahead	8%	31%	**42%**	19%
2-hour ahead	22%	20%	**38%**	20%
3-hour ahead	25%	13%	**45%**	16%
4-hour ahead	29%	20%	**38%**	13%
Winter	20%	22%	**38%**	20%
Spring	15%	25%	**40%**	20%
Summer	24%	17%	**47%**	12%
Fall	25%	23%	**38%**	14%
Boulder	27%	15%	**43%**	15%
Bondville	21%	21%	**35%**	23%
Goodwin Creek	21%	23%	**39%**	17%
Fort Peck	23%	**31%**	**31%**	15%
Desert Rock	15%	31%	**42%**	12%
Penn State	25%	15%	**45%**	15%
Sioux Falls	15%	12%	**50%**	23%
All Situations	20.8%	21.1%	**41.1%**	17.0%

Table 3: Relative Frequencies of ML Models per MAE Metric

Forecast Situation	RF	SVM	ANN	GBM
1-hour ahead	7%	**65%**	17%	11%
2-hour ahead	15%	**44%**	26%	15%
3-hour ahead	14%	**36%**	**36%**	14%
4-hour ahead	23%	**32%**	26%	19%
Winter	17%	**41%**	25%	17%
Spring	6%	**60%**	19%	15%
Summer	21%	**38%**	25%	16%
Fall	12%	**40%**	35%	13%
Boulder	10%	**48%**	25%	17%
Bondville	8%	**52%**	17%	13%
Goodwin Creek	23%	**35%**	19%	23%
Fort Peck	21%	**42%**	27%	10%
Desert Rock	21%	**48%**	19%	12%
Penn State	8%	**42%**	40%	10%
Sioux Falls	10%	**44%**	27%	19%
All Situations	14.6%	**44.3%**	26.2%	14.9%

Appendix C: Figures

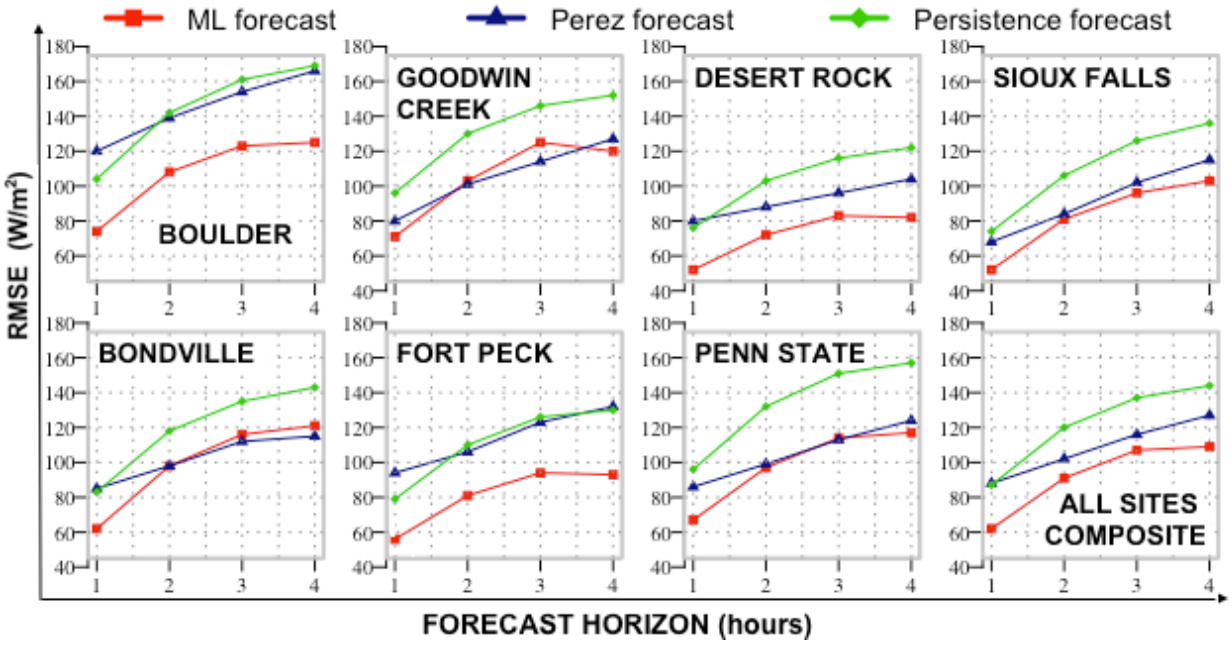

Figure 1: ML and benchmark methods' performances forecasting different forecast horizons.

VII. REFERENCES

[1] D. Lew, D. Piwko, N. Miller, G. Jordan, K. Clark, and L. Freeman, *How do high levels of wind and solar impact the grid? The western wind and solar integration study,* National Renewable Energy Laboratory Technical Report. **303,** (2010).

[2] R.H. Inman, H.T.C. Pedro, and C.F.M. Coimbra, *Solar forecasting methods for renewable energy integration,* Progress in Energy and Combustion Science. **39** (6), 535-576 (2013).

[3] E. Lorenz, D. Heinemann, H. Wickramarathne, H.G. Beyer, and S. Bofinger, *Forecast of ensemble power production by grid-connected PV systems,* in *20th European PV Conference.* 2007. Milano.

[4] H.T. Pedro and C.F. Coimbra, *Assessment of forecasting techniques for solar power production with no exogenous inputs,* Solar Energy. **86** (7), 2017-2028 (2012).

[5] R. Marquez, V.G. Gueorguiev and C.F. Coimbra, *Forecasting of global horizontal irradiance ausing sky cover indices,* Journal of Solar Energy Engineering. **135** (1), 011017 (2013).

[6] A. Mellit, H. Eleuch, M. Benghanem, C. Elaoun, and A. Massi Pavan, *An adaptive model for prediction of global, direct and diffuse hourly solar irradiance,* Energy Conversion and Management. **51** (4), 771-782 (2010).

[7] W. Ji and K.C. Chee, *Prediction of hourly solar radiation using a novel hybrid model of ARMA and TDNN,* Solar Energy. **85** (5), 808-817 (2011).

[8] D. Yang, P. Jirutitijaroen, and W.M. Walsh, *Hourly solar irradiance time series forecasting using cloud cover index,* Solar Energy. **86** (12), 3531-3543 (2012).

[9] R.H. Inman, H.T.C. Pedro, and C.F.M. Coimbra, *Solar forecasting methods for renewable energy integration,* Progress in Energy and Combustion Science. **39** (6), 535-576 (2013).

[10] R. Perez, S. Kivalov, J. Schlemmer, K. Hemker Jr., D. Renne, and T.E. Hoff, *Validation of short and medium term operational solar radiation forecasts in the US,* Solar Energy. **84** (12), 2161-2172 (2010).

[11] G. Reikard, *Predicting solar radiation at high resolutions: A comparison of time series forecasts,* Solar Energy. **83** (3), 342-349 (2009).

[12] R.E. Bird and R.L. Hulstrom, *Simplified clear sky model for direct and diffuse insolation on horizontal surfaces,* Solar Energy Research Inst., Golden, CO. 2013.

[13] R. Marquez, V.G. Gueorguiev and C.F. Coimbra, *Forecasting of global horizaontal irradiance ausing sky cover indices,* Journal of Solar Energy Engineering. **135** (1), 011017 (2013).

[14] R. Perez, S. Kivalov, J. Schlemmer, K. Hemker Jr., D. Renne, and T.E. Hoff, *Validation of short and medium term operational solar radiation forecasts in the US,* Solar Energy. **84** (12), 2161-2172 (2010).

[15] P. Mathiesen,and J. Kleissl, *Evaluation of numerical weather prediction for intro-day solar forecasting in the continental United States,* Solar Energy. **85** (5), 967-977 (2011).

[16] De Giorgi, M.G., P.M. Congedo, M. Malvoni, and D. Laforgia, *Erro analysis of hybrid photovoltaic power forecasting models: A case study of mediterranean climate,* Energy Conversion and Management. **85,** 117-130 (2015).

[17] Y. Chu, M. Li, H.T.C. Pedro, and C.F. Coimbra, *Real-time prediction intervals for intra-hour DNI forecasts,* Renewable Energy. **83**, 234-244 (2015).

[18] Y. Zhang and Z. Hamidreza, *Day-ahead power output forecasting for small-scale solar photovoltaic electricity generators,* IEEE Transactions On Smart Grid. **6** (5), 2253-2262 (2015).

[19] K. Hornik, M. Stinchcombe, and H. White, *Multilayer feedforward networks are universal approximators,* Neural Networks. **2** (5), 359-366 (1989).

[20] C. Cornaro, M. Pierro, and F. Bucci, *Master optimaization process based on neural networks ensemble for 24-h solar irradiance forecast,* Solar Energy. **111**, 297-312 (2015).

[21] Y. Chu, M. Li, H.T.C. Pedro, and C.F. Coimbra, *Real-time prediction intervals for intro-hour DNI forecasts,* Renewable Energy. **83**, 234-244 (2015).

[22] M. Abuella and B. Chowdhury, *Random forest ensemble of support vector regression for solar power forecasting,* in *Proceedings of Innovative Smart Grid Technologies, North American Conference.* 2017.

[23] H. Zheng and A. Kusiak, *Prediction of wind farm power ramp rates: A data-mining approach,* Journal of Solar Energy Engineering. **3** (3), 031011 (2009).

[24] M. Zamo, O. Mestre, P. Arbogast, and O. Pannekouche, *A benchmark of statistical regression methods for short-term forecasting of photovoltaic electricity production, part I: Deterministic forecast of hourly production,* Solar Energy. **105**, 792-803 (2014).

[25] J.H. Friedman, *Greedy function approximation: a gradient boosting machine,* Annals of Statistics. 1189-1232 (2001).

[26] J. Zhang, et al., *A suite of metrics for assessing the performance of solar power forecasting,* Solar Energy, **111**, 157-175 (2015).

[27] R. Perez, S. Kivalov, J. Schlemmer, K. Hemker Jr., D. Renne, and T.E. Hoff, *Validation of short and medium term operational solar radiation forecasts in the US,* Solar Energy. **84** (12), 2161-2172 (2010).